

Thermal modeling of space debris via Finite Element Analysis

Paul McCall

Florida International University, Miami, Florida

Rachel Sharples

Schafer Corporation, Albuquerque, New Mexico

Dr. Jean H. Andrian, Dr. Armando Barreto, Dr. Naphtali Rische, and Dr. Malek Adjouadi

Florida International University, Miami, Florida

ABSTRACT

The study of space debris is of critical importance to all space-faring nations. The characterization of debris objects through means of passive imaging techniques would allow for further studies into the origination, specifications, and future trajectory of debris objects. The long-wave infrared waveband is a potential candidate for the observation of space debris. However, in order to simulate and study the radiance of these objects on long-wave infrared detectors, assumptions have to be made regarding the radiative energy incident upon the object, which determines the temperature of the object. The purpose of this investigation is to study the steady-state radiative thermal equilibrium temperature, temperature transients, and object temperature as a function of time, for varying cuboid-type space debris objects. Conclusions are made regarding the aforementioned thermal analysis as a function of debris orbit, geometry, orientation with respect to time, and material properties.

1.0 INTRODUCTION

Space debris has long been a problem for the United States as well as other space-faring nations. The proliferation of space debris in the last decade has brought us closer to dealing with such problems through means of active debris removal. The U.S. Space Surveillance Network tracks over 22,000 pieces of debris 10cm or larger [1]. However, experts believe there to exist many times this amount of debris that cannot be tracked or detected due to its size, material properties, and orbit. The characterization of space debris is important because an understanding of the structure, mass, and material properties may help researchers to further extract needed information regarding the orbit and origination of such debris. To this end the broad scope of this research is focused on the Long-wave Infrared (LWIR) signatures of space debris. In order to calculate and model the LWIR signatures of such debris in orbits between low-Earth orbit and geosynchronous orbit, a representative and accurate thermal model must be developed.

Long-wave infrared imaging techniques offer many potential benefits when applied to the remote sensing of space debris. LWIR imaging technologies may allow for the imaging of objects with the Sun in the field-of-view without saturation of the imaging system. Imaging space objects in the LWIR band has the inherent advantage of not being dependent upon Solar or Earth illumination which makes the observations and measurements possible even when observed objects are in eclipse. This temperature and wavelength dependence is expressed in Planck's equation for blackbody radiation, which is shown in Equation 1 [2]. The spectral radiance of a blackbody is dependent upon the waveband of interest and the temperature of the emitting object. Therefore if one is concerned with the imaging of objects in the LWIR band, the model, assumptions, analyses, and processes leading to the determination of the object temperature need to be accurate and understandable.

$$L(\lambda, T) = \frac{2hc^2}{\lambda^5} \frac{1}{e^{\frac{hc}{\lambda kT}} - 1} \quad \left[\frac{\text{Watts}}{\text{m}^2 \text{ m sr}} \right] \quad (1)$$

The thermal analysis described here takes into account the specific orbit, size, orientation, rigid body structure, and material properties of simulated debris. Approximations for the rigid bodies of space debris are comprised of cuboids, cylinder, plates, and rocket bodies. The steady-state section of this analysis calculates the radiative equilibrium temperatures of debris due to the radiation emitted by the Sun as well radiation emitted by the Earth.

In the area of space debris research there exists little data regarding the temperatures of debris in orbit with respect to time [3]. As each face of the debris object will be receiving heat flux at a different rate during orbit, the problem cannot be simplified to a one- or two-dimensional analysis. Determining the three-dimensional thermal profile of the debris while considering the effects of received radiant flux, radiation from the debris out to space, and conduction of heat through the debris material in all three dimensions results in a set of partial differential equations with respect to three variables that cannot be solved analytically but can be approximated using the method of Finite Element Analysis (FEA). Finite element analysis will be used further for the transient analysis, adding specific material specifications such as conduction and emission properties, in order to approximate the thermal transients of debris. Such transient scenarios would occur where debris passes through eclipse due to its orbit, which is representative of much of the debris in low-Earth orbit.

2.0 METHODS

There are two main components inherent to the thermal modeling described in this paper: 1) the definition and calculation of the radiance profiles and 2) the insertion of this data into the Finite Element Analysis software package in SolidWorks.

2.1 RADIANCE PROFILES

The derivation of the radiance profile that is experienced by the orbiting debris object is a function of the debris orbit, geometry, orientation with respect to time, and material properties. An overview of this process is outlined, with a detailed explanation of each step in the following paragraphs.

The normalized vectors from the debris object to the Earth and the Sun are calculated for all points along the debris object's orbital path. The debris object is then given a three-dimensional geometry, or rigid body structure, along with a specified tumble rate and tumble direction. Once the geometry of the debris object and the orientation of the debris solid body relative to the local coordinate system are known, the normalized vectors for all sides of the debris object can be determined. Assumptions are made regarding the size, distance, and radiating temperature of the Earth and Sun. With a known range, angular subtends, and radiating temperature, the radiant flux density incident upon the point in space which the debris object occupies along its orbital track can be calculated. The normalized vectors for all sides of the debris object, their orientation relative to that of the Earth and Sun, and the irradiance due to the Earth and Sun on a specific point in three-dimensional space where the debris object is located are all known. Therefore, the projected area receiving radiation and the amount of radiative energy the projected area is receiving, from the Sun and/or Earth can be determined for all sides as a function of time for all points along the orbital path of the debris object.

The first step in the calculation of the radiance profiles is to determine the vectors stemming from the center of the debris object and pointing towards the Sun and the Earth. These vectors are determined relative to an Earth-centered coordinate system. The vectors are calculated in 10-second increments for one entire orbital period. Contained within the vectors is the range from the object to the Sun and to the Earth. The vectors data can be created in MATLAB [4] or exported from simulation scenarios modeled in Systems Tool Kit 10 (STK 10) [5].

After the Earth and Sun vectors have been calculated, the debris object is given a three-dimensional solid body representation, a tumble direction, and accompanying tumble rate. For the simulations contained in this paper, the debris object three-dimensional solid body is constrained to a cuboid structure of varying size and mass. The cross-sectional areas, construction, tumble directions, and tumble rates used to specify the debris objects to be simulated are described in Table 1. The orbital characteristics of the simulated debris object are shown in Table 2.

Table 1. Geometric and tumble constraints used for simulation

| Side Area [cm] | Debris Construction | Tumble Direction | Tumble Rate [rpm] |
|----------------|---------------------|-----------------------|-------------------|
| 10 | Solid | Spin about Nadir axis | 0.01 |
| 17 | Hollow | | 0.1 |
| | | | 1 |

Table 2. Debris object orbital characteristics

| Orbital Type | Semi-major Axis | Eccentricity | Inclination | Orbital Period [min] | Propagator |
|---------------------|-----------------|--------------|-------------|----------------------|------------|
| Circular - Prograde | 7278.14 km | 0 | 98° | 102.9 | J2 |

The tumble rate and tumble direction are specified with a yaw and pitch angular offset relative to the local coordinate frame. These specifications establish the initial conditions for the orientation of the front face of the orbital debris. Once the orientation of the front face is established, the normalized vectors for each face, or side, of the debris can be determined since the object is of a cuboid geometry. Assumptions regarding the distance, size, and radiating temperature of the Earth and Sun are made. These values are shown in Table 3.

Table 3. Earth and Sun constants used for simulations

| Temperature – Sun [K] | Temperature – Earth [K] | Radius of Earth [km] | Earth Albedo | Astronomical Unit [km] | Solar Constant [W/m ²] |
|-----------------------|-------------------------|----------------------|--------------|------------------------|------------------------------------|
| 5778 | 254 | 6,371 | 0.306 | 149,597,871 | 1368 |

Classically, the Sun is assumed to operate as a point source in regard to the Earth-centered orbits that are simulated in this research. Equation 1 represents the radiant flux density due to the Sun at Earth-orbit [6]. The distance to the Sun remains relatively constant and is set to 1 AU. This is expressed as the parameter ‘D’ in Equation 1. The distance from the Earth-orbiting debris object can be dynamic and is determined as previously mentioned with the extracted vectors data from STK 10. Due to the relative proximity of the Earth to the debris object, the Earth cannot be assumed to operate as a point source. Instead the Earth is modeled as an extended area source. With the Earth being modeled as an extended area source, the amount of the Earth’s surface that will radiate energy to the debris object is dependent upon the height of the object above the surface of the Earth. This relationship is demonstrated through the Earth depression angle, α_e , expressed in Equation 2 where the ‘r’ represents the radius of the Earth and ‘x’ represents the orbital altitude of the debris object above the Earth’s surface [6].

$$SC = \frac{4\pi * R_{Sun}^2 * \sigma * T_{Sun}^4}{4\pi * D^2} \quad \left[\frac{\text{Watts}}{\text{m}^2} \right] \quad (1)$$

$$\alpha_e = \cos^{-1} \left(\frac{r}{r + x} \right) \quad \left[\frac{\text{Watts}}{\text{m}^2} \right] \quad (2)$$

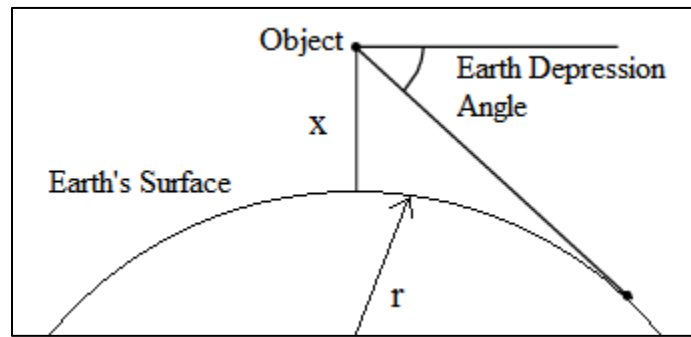


Figure 1. Earth depression angle

Figure 1 demonstrates the relationship between Earth depression angle and subtended field-of-view as a function of orbital altitude above Earth’s surface. As the distance between the Earth’s surface and the object decreases, the amount of surface area of the Earth which radiates energy to the object will also decrease. As a result the amount of radiated energy from the Earth to the debris object will not simply be a function of range and temperature of the Earth but will include the amount of the Earth’s surface area re-radiating energy to the object as well.

The surface of the Earth is modeled as a composite of eight quarter-spheres. A quarter-sphere is shown in Figure 2 and is constructed by dividing a hemi-sphere into four equal parts. The quarter-sphere is comprised of an aggregate of Lambertian radiators [2]. Each radiator has a given surface area representing the emitting area of that region of the Earth's surface and the radiating temperature indicated in Table 3. Once the quarter-sphere is modeled, the distance from the debris object to each radiator and the angle between each radiator normal vector and the debris object are calculated. The irradiance from the Earth to any point in space can be calculated using Equation 3 and is expressed in Watts per meter squared [6]. The ' A_{rad} ' parameter in Equation 3 represents the projected surface area of the Earth which is radiating energy to the debris object according to the Earth depression angle.

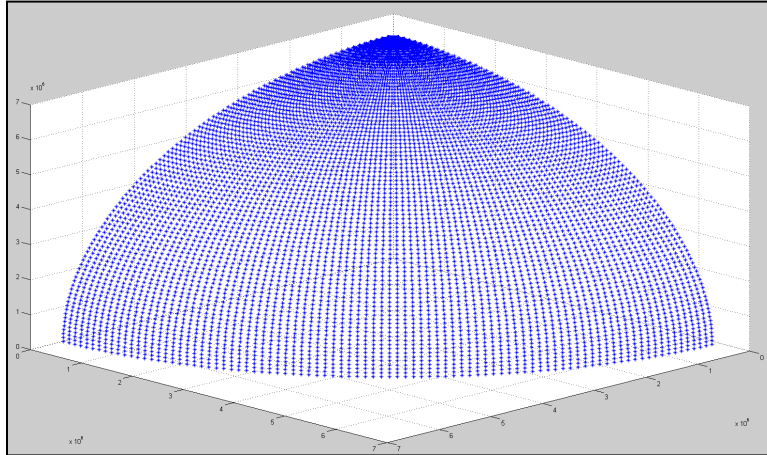


Figure 2. Earth quarter-sphere

$$I_{Earth} = (1 - a_{earth}) * \frac{A_{rad} * \sigma * T_{earth}^4}{2\pi * D^2} \quad \left[\frac{\text{Watts}}{\text{m}^2} \right] \quad (3)$$

Equations 1 and 3 represent the irradiance at a point in space due to the Sun and Earth. However, this is not equivalent to the radiant flux experienced by the orbital debris occupying that point in space. The radiant flux incident upon the orbital debris will depend upon the attitude of the object as a function of time along the orbital path of the debris object. The received radiant flux for each side of the debris object is determined by calculating the dot product of the normal vector from each face of the debris object with the Earth and Sun vectors. The resultant dot product is used as the projected area of each face of the cuboid debris object that is receiving radiation from the Sun and/or the Earth. The radiant flux profiles for every side of the object can be determined utilizing the calculated radiant flux densities from the Earth and Sun on the object using Equations 1 and 3 and the projected area of the debris object that is receiving radiation from the Sun and the Earth. The total radiant flux incident on each face of the debris object is expressed in Equation 4 [6]. The ' $\cos \gamma$ ' and ' $\cos \delta$ ' terms represent the dot product calculation of the normal vector for each face with the vectors from the debris object to the Earth and the Sun respectively. The total radiant flux on each face ' Φ_{Total} ' is expressed in Watts.

$$\Phi_{Total} = I_{Earth} * \cos \gamma + SC * \cos \delta \quad [\text{Watts}] \quad (4)$$

2.2 FINITE ELEMENT ANALYSIS

To begin building a simulation-based database of temperature profiles of debris in orbit, the FEA-based thermal simulation tool in SolidWorks was used to simulate the temperature of cuboid structures representing a small part of the debris tradespace. Results and conclusions drawn from these simulations will be used to justify simplifications that make simulating a much larger part of the entire debris tradespace more feasible.

The first set of FEA simulations examined the thermal profile of a cuboid geometry with respect to time. A 10cm hollow cube with a 5mm shell, a 17cm hollow cube with an 8.5mm shell, and a 10cm solid cube were exposed to the heat flux produced from a nadir-pointing circular orbit in LEO, as mentioned in Table 3. Note that the 17cm cube with an 8.5mm shell is simply scaled up from the 10cm cube with a 5mm shell. Each cuboid geometry was

simulated with three in-orbit tumble rates: 0.01, 0.1, and 1.0 revolutions per minute. In addition to the effects of the orbit on the thermal profile, the simulations also examined the effect of overall mass, the absorptivity-to-emissivity (α/ϵ) ratio, and the mechanical thermal properties of different materials on each cube's thermal profile.

Aluminum 7075 was chosen as the initial material for simulation, since it is a common material used in CubeSat structures. CubeSat aluminum structures are also often chromanodized, so the emissivity and absorptivity values were set to 0.56 and 0.44, respectively, which represent chromanodized aluminum [7]. A separate set of simulations with emissivity of 0.56 and absorptivity of 1.0 were also run to determine the effect of increased absorptivity-to-emissivity ratio on the thermal profile. (Note that the second set of values for absorptivity and emissivity are not realistic, as $\alpha + \epsilon$ should sum to 1.) These values and ratios are listed in Table 4.

Table 4. Absorptivity and emissivity values for chromanodized comparative coating

| Property | Chromanodized Value | Comparison Value |
|---------------------------|---------------------|------------------|
| Emissivity (ϵ) | 0.56 | 0.56 |
| Absorptivity (α) | 0.44 | 1.0 |
| α/ϵ | 0.79 | 1.79 |

The chromanodized absorptivity/emissivity ratio was also applied to titanium, along with two purely theoretical materials: Al-7075 with the specific heat (c_p) of titanium and Al-7075 with the conductivity (k) of titanium. The goal of simulating these three additional materials is to first isolate the effects of different specific heat and conductivity values on the overall thermal profile and then to examine the combined effects of these two mechanical thermal properties in a realistic material. Table 5 summarizes the materials used along with their thermal and material properties.

Table 5. Thermal and material properties used for simulations

| Material | $c_p \left[\frac{J}{kg * K} \right]$ | $k \left[\frac{W}{m * K} \right]$ | $\rho \left[\frac{kg}{m^3} \right]$ | α/ϵ |
|-------------|---------------------------------------|------------------------------------|--------------------------------------|-------------------|
| Al-7075 | 960 | 130 | 2810 | 0.79, 1.79 |
| Al7075_cpTi | 520 | 130 | 2810 | 0.79 |
| Al7075_kTi | 960 | 16.4 | 2810 | 0.79 |
| Titanium | 520 | 16.4 | 4510 | 0.79 |

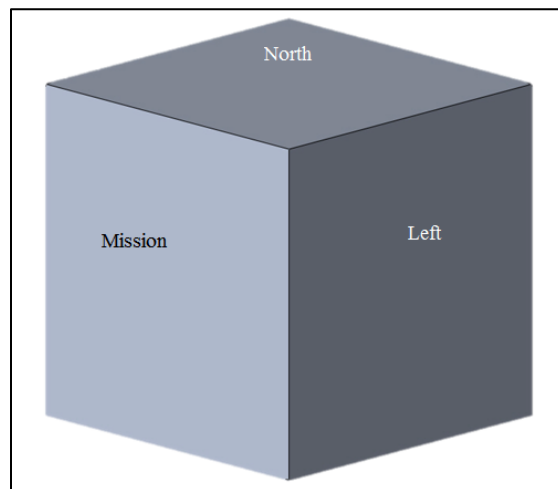


Figure 3. Solid model rendering of a cube

A solid model of the cuboid geometry as rendered in SolidWorks is shown in Figure 3. The Mission, anti-mission, right, left, north, and south faces were assigned to the cube according to convention for application of the orbit-determined heat flux.

The radiance profiles described in the previous section were used to create a database of face-by-face heat flux profiles in SolidWorks. Each face had an individual heat flux profile of 8641 points with a time step of 10 seconds in between each point that was uploaded to that face from the database. Since the heat flux profiles are based on the geometry of orbit, in this way orbit was simulated for each object. SolidWorks, however, will only allow 5000 points at a time in any heat flux profile in the database. To fit into the database format, the 8641-point profiles were split into two separate files, one 5000 points long and the other 3641 points long. When the first simulation was complete (up to 49990 seconds) using the first 5000 points, the thermal profile from the final time step was used as the initial thermal profile for a new simulation that would cover the remaining 3641 points. For objects that took longer than 86410 seconds to reach steady state, the heat flux profile was repeated—i.e., another simulation using the final time step's thermal profile (point 3641) as the initial thermal profile was run with the heat flux profile starting over for the first 5000 points. Absorptivity of the object is also a parameter set during this part of simulation set-up. This process was repeated until the object had achieved steady state.

All six faces were set to radiate surface-to-ambient to 77K, which is the standard ambient radiation temperature in Time-domain Analysis Simulation for Advanced Tracking (TASAT), with the desired emissivity value as discussed previously. In addition, the entire object was set to an initial temperature of 77K. However, one limitation of SolidWorks is that initial temperature values can only be set on the surfaces of an object, not throughout the entire object. To create this initial temperature profile, all six faces were set to 77K and run to steady state without a transient analysis, thus creating a 77K temperature profile throughout the entire object. The result of this simulation was set as the initial thermal profile of the first transient simulation as the initial thermal condition.

All simulations used a time step size of 10 seconds and were run with a coarse mesh and SolidWorks' FFEPlus iterative solver. Figure 4 shows the coarse mesh over a 10cm cube. Simulations were run and their final thermal profiles fed into the next simulation as the new initial thermal profile, thus keeping continuity from one simulation to the next and allowing for longer simulations to be run than the heat flux profile size limitations would allow, until the object reached steady state.

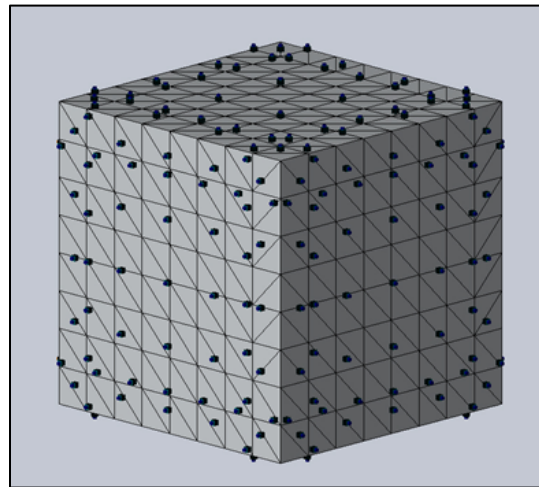


Figure 4. Coarse finite element mesh applied to hollow 10cm cube in SolidWorks

Each simulation produces a comprehensive set of results. It is possible to pull the temperature from any element at any 10-second time step. The software can also calculate the maximum, minimum, and bulk temperature with respect to time for any surface of the object. For this study, only the bulk temperature of the mission, anti-mission, and north faces with respect to time were used.

One way that SolidWorks Simulation presents results is a visual representation of the temperature gradient of the object at any single time step of the simulation. An example of this type of thermal profile for a 10cm hollow cube with absorptivity 0.44 and tumble rate 1.0 rpm is shown in Figure 5.

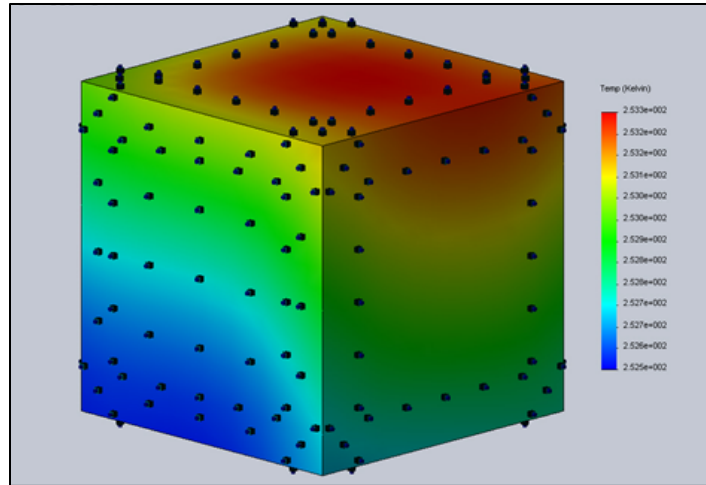


Figure 5. Thermal profile at time 49990 seconds for a 10cm Al-7075 hollow cube with absorptivity 0.44 in a circular, nadir-pointing orbit with a 1.0 rev/min tumble rate at LEO

The thermal profiles from each time step can also be put together as an animation demonstrating shifts in the temperature gradient. For this paper, SolidWorks was used to calculate the bulk temperature of each face with respect to time. This information was exported as a .csv file containing the time step, the time in simulation, and the calculated temperature. These files were then read into MATLAB for processing. If a simulation required more than one run, the file from each run for each face would be loaded separately and then plotted on a single graph for each face to check for continuity between time segments. The steady state portion of the data was then isolated by face. Figure 6 shows the points used in this process for a chromanodized Al-7075 10cm hollow cube with a tumble rate of 0.01 rpm.

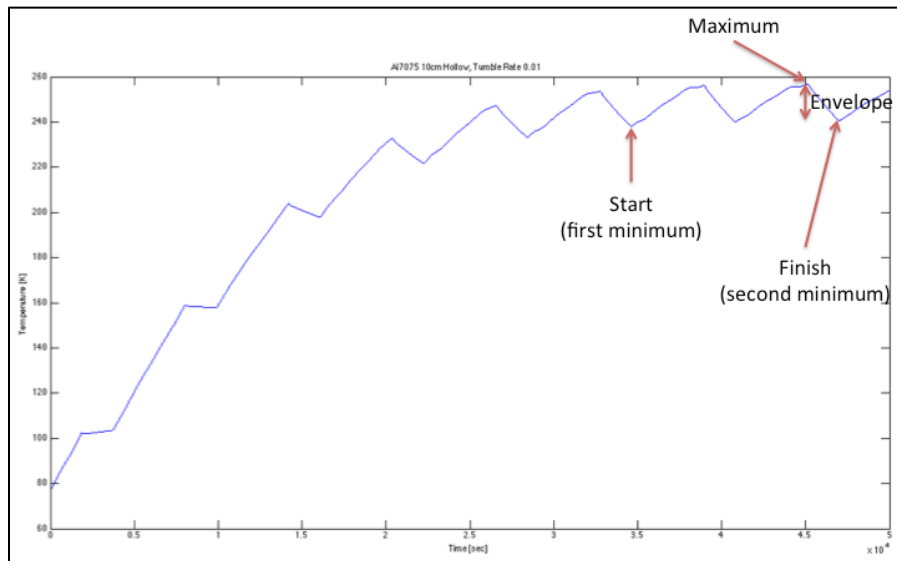


Figure 6. Key points in steady-state analysis

The value and time of the first and last minimum temperatures after steady state were recorded to ensure that the steady state average was taken after n complete cycles and not mid-cycle. The steady-state average between these two minima was then calculated using MATLAB's average function. Once the average had been calculated for the

mission, anti-mission, and north faces, the standard deviation between the three faces was also calculated using the STDEVP function in Excel. The value and time of the last maximum temperature between the two minima were also recorded. The final minimum was subtracted from the maximum to yield the thermal envelope.

3.0 RESULTS

The results contained within this paper are focused on analyzing the dependency of certain orbital debris specifications such as size, material, geometry, tumble rate, and thermal properties on the temperature profile of the debris object with respect to time for three faces (Mission, Anti-Mission, and North) of the debris object. An example is shown in Figure 7 illustrating the temperature of three faces of an object for fixed material specifications and debris geometry with differing tumble rates.

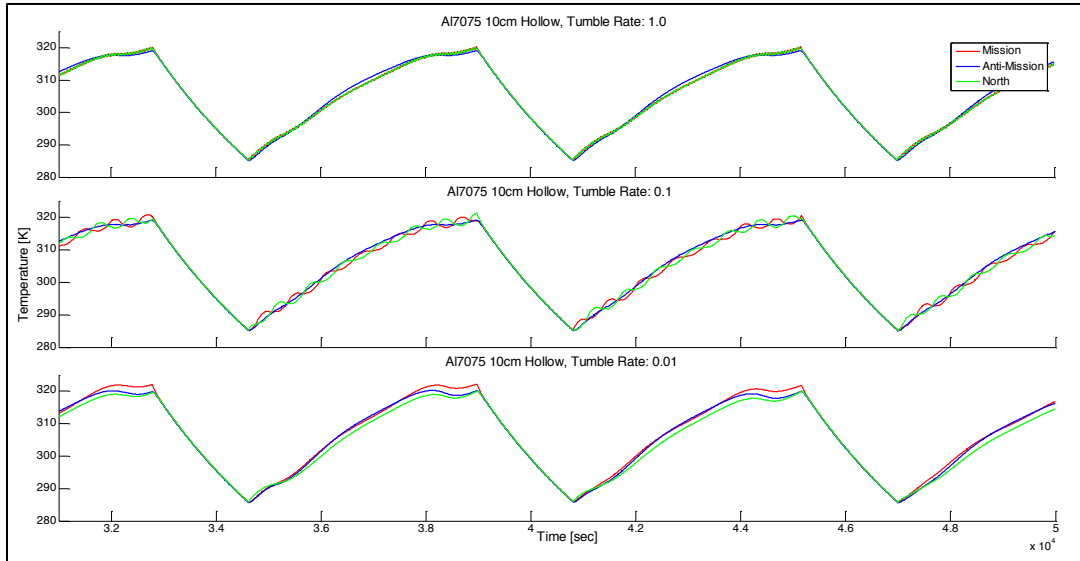


Figure 7. Temperature profiles versus time for multiple faces and tumble rates

From simulations, Figure 8 shows the radiative thermal equilibrium (RTE) temperature is minimally dependent upon the size and mass of an object. Figure 8 shows steady-state simulations for Al-7075 and titanium, along with two purely theoretical materials: Al-7075 with the specific heat of titanium, and Al-7075 with the conductivity of titanium. Analysis of the 'Al-075' case shows that for all debris geometries simulated, the difference in RTE is less than 1K. For the 'Titanium' case the difference between maximum and minimum RTE for debris geometries simulated is less than 3K. The RTE profiles for the debris geometries are notably different for the two hypothetical materials. The 'Al7075_cpTi' case, Al-7075 with the specific heat of titanium, yields the same RTE values for the 10 cm solid and the 17 cm hollow debris geometries; however there is a 1.5K increase in the RTE of the least-massive debris object, the 10 cm hollow case. The 'AL7075_kTi' case, Al-7075 with the conductivity of titanium, replicates the 'Titanium' RTE profile with the exception that the RTE temperatures have decreased by 1K. Figure 9 demonstrates that different materials may experience different temperature values for their steady-state RTE; however the size and mass of the debris object itself has little effect on the RTE of the debris object. The maximum temperature gradient within a material simulation occurs in the 'Titanium' case and is less than 3K.

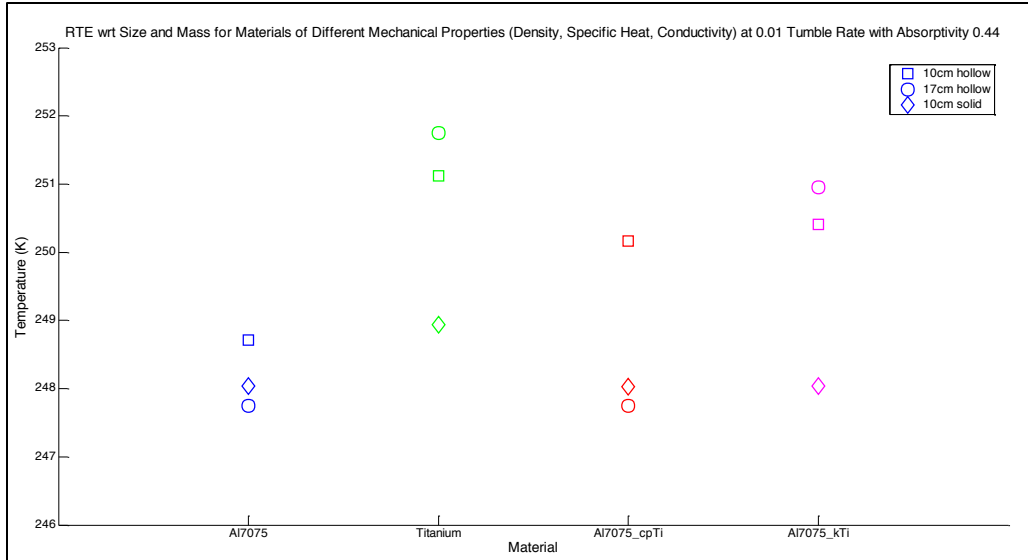


Figure 8. RTE of varying materials for differing size and mass debris objects

Figure 9 shows the simulation results for three different debris geometries while modulating the absorptivity values for the Al-075 material. This is done in order to investigate the effect that absorptivity and debris geometry have on the RTE temperature and time to reach steady-state. It can be seen that all debris geometries simulated with absorptivity equal to 0.44 reach RTE at 248K +/- 1K. The same debris geometries simulated with absorptivity equal to 1.0 reach RTE at 304K +/- 2K. In accordance with the findings expressed in Figure 8, Figure 9 also shows that debris geometry has little effect on the variance of the RTE for a given material. Instead the RTE reached by debris is more dependent on the absorptivity-to-emissivity ratio than on the debris geometry. A material with a higher absorptivity-to-emissivity ratio will reach a higher RTE temperature because it is absorbing radiation at an increased rate relative to materials with lower absorptivity-to-emissivity ratios. Further analysis into Figure 9 demonstrates that the more massive an object is, and the lower its absorptivity value is, the longer it will take to reach its steady-state RTE temperature.

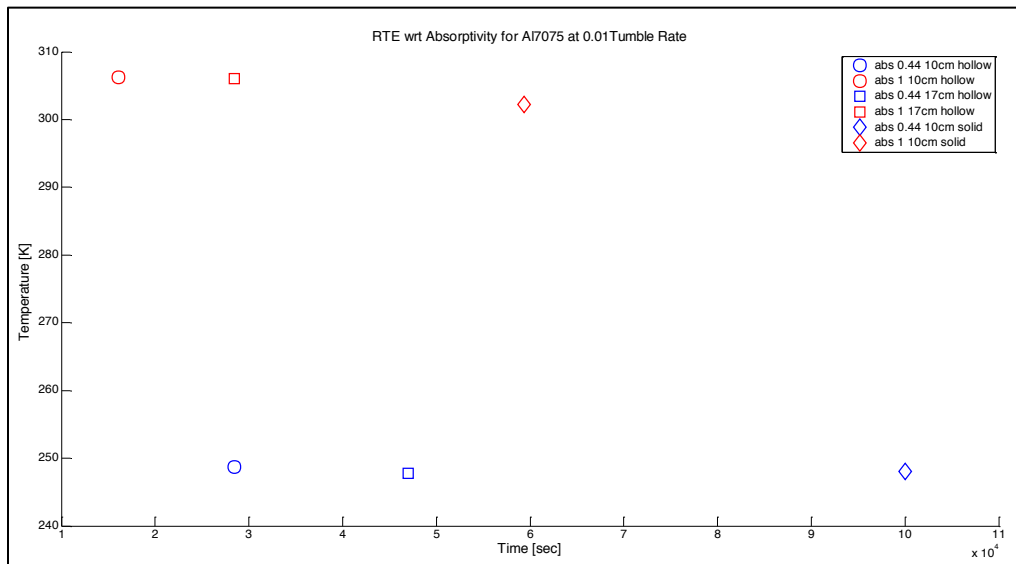


Figure 9. Time to steady-state and RTE temperature for varying absorptivity values and debris geometries

Analysis was carried out regarding the tumble rate of orbital debris and its effect on RTE temperature. These results are shown in Figure 10. The Al7075 material was simulated for a 10 cm hollow and solid cube having absorptivity

values of 0.44 and 1 for three tumble rates: 0.01, 0.1, and 1 rpm. The data points shown in the top subplot of Figure 10 are broken out into the bottom three subplots to show detail along the time and temperature axis. Regardless of tumble rate, analysis of the top subplot of Figure R3 leads to findings that are similar to that of Figure 9; RTE temperature reached and time to steady-state are dependent upon the mass and absorptivity of a certain debris object. When analyzing the data points representing the different tumble rates in the bottom three subplots, the RTE temperature reached for a given simulation varies by less than 1.5K, while the time to steady state varies by less than 10 seconds.

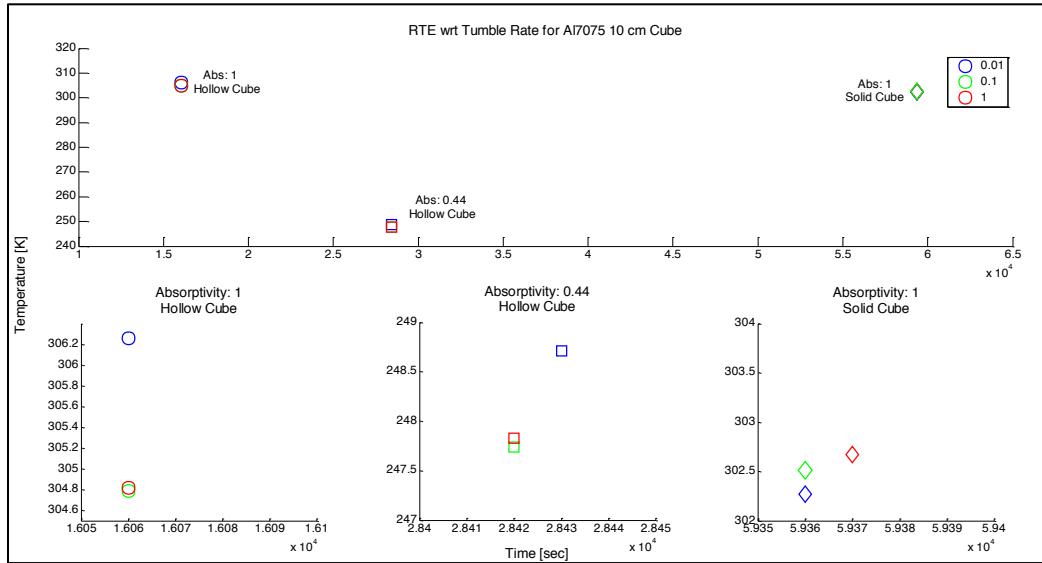


Figure 10. RTE versus tumble rate for Al-7075 10 cm

The last aspect of this analysis is concerned with the temperature deviations experienced by the debris object from one face to another. Figure 11 analyzes the RTE temperature versus time to steady state for the different faces of the cuboid debris object. The top and middle subplots in Figure 11 shows the data points for three faces of the debris geometry for all three debris geometries simulated. The top subplot utilizes titanium for the simulation material with a given absorptivity and tumble rate, while the middle subplot utilizes Al-7075 for the simulation material with a given absorptivity and tumble rate. The maximum temperature gradient between faces, 8K, occurs in the titanium simulation for the 17 cm hollow debris geometry. All inter-face temperature gradients for the Al-7075 simulation are less than 1K. For both materials, the inter-face temperature gradient decreases as the faces become less thermally independent. For fixed material specifications, the smaller and the more solid an object is, the more thermally dependent one face will be on another, therefore decreasing the inter-face temperature gradient. Heat energy will be able to transfer more easily due to the increased amount of thermally conductive connections and decreased distance between faces. The inter-face thermal gradients will be larger for the titanium relative to the Al-7075 due to the decreased thermal conductivity of the titanium. The three subplots on the bottom row of Figure 11 show the RTE temperature for an object with fixed material specifications and debris geometry for all three tumble rates. The inter-face thermal gradient for each tumble rate is less than 1K. These findings are also supported by Figure 12 which shows the temperatures with respect to time for three of the six faces of the cuboid debris object. The disparity between face temperatures is greatest for the 17 cm hollow titanium simulation in the top left subplot. As the debris object becomes smaller and more solid (the right-most subplots), the disparity between face temperatures decreases. This transition to a more solid object is accompanied by a decreasing thermal envelope. In addition, as the material's thermal conductivity increases (the bottom subplots), the disparity between face temperatures decreases as well.

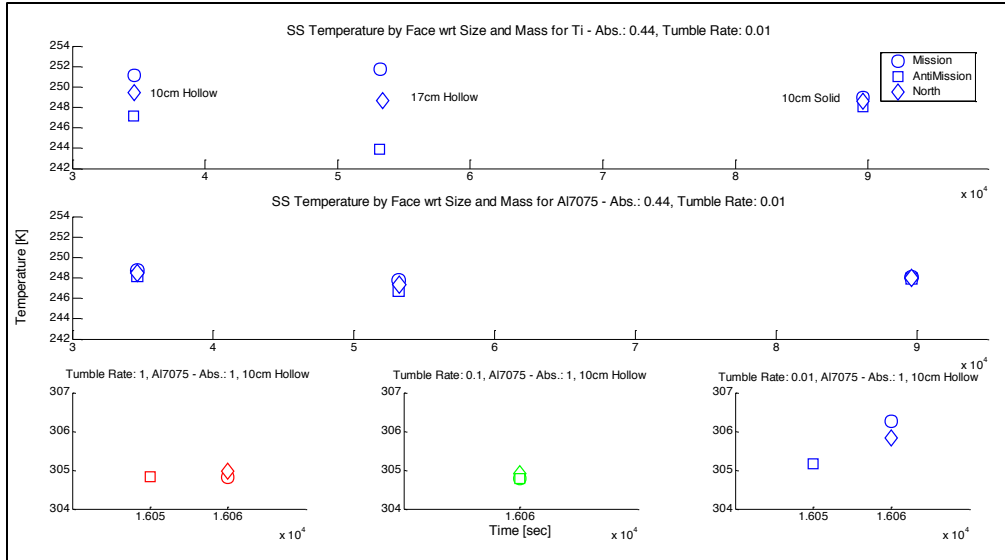


Figure 11. Time to steady-state and RTE temperature of multiple faces

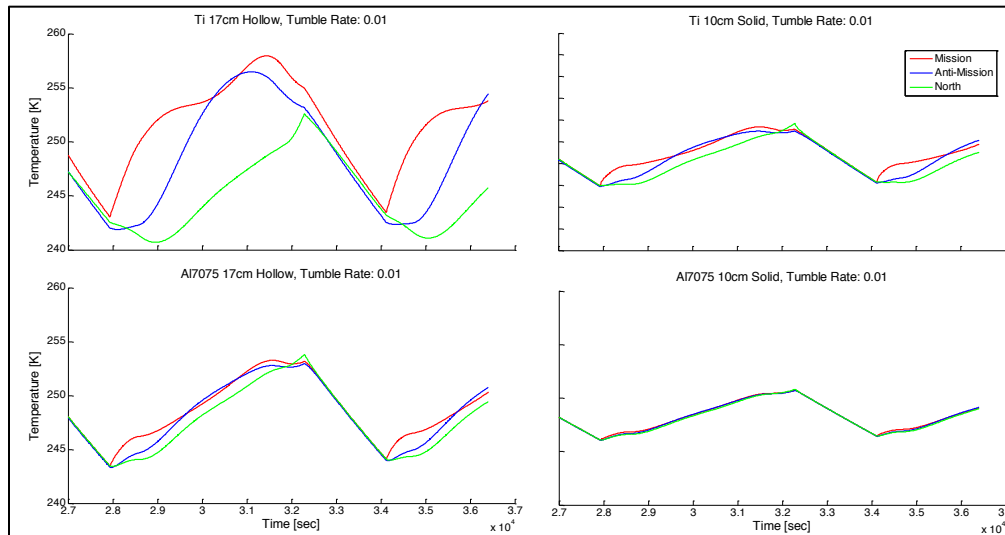


Figure 12. Temperature profile by face for varying material, size, and mass debris objects

4.0 CONCLUSIONS AND FUTURE WORK

Debris objects were modeled with differing materials utilizing both real and hypothetical values for their material and thermal properties for this investigation. The radiance profile was calculated for each face of the cuboid debris object which was simulated in a polar low-Earth orbit. The radiance profile calculated takes into account the radiation emitted from both the Sun and the Earth on the debris object. The radiance profiles are then subjected to finite element analysis utilizing the specified debris geometry, resulting in temperature profiles for each face of the object. These temperature profiles were analyzed and the following conclusions made.

The radiative thermal equilibrium (RTE) temperature of an object seems to be a function of material properties, solar absorptivity and emissivity, and is independent of size (10 cm case versus 17 cm case), or mass (hollow versus solid objects). Larger, more massive objects will reach the same RTE as less massive objects with similar properties. However the larger, more massive objects will take longer to reach their RTE. More massive objects will experience a decreased thermal envelope because they will heat up and cool down more slowly than similar, less massive, objects. Faces of a simulated cuboid debris object appear to approach the RTE temperature of the object throughout

simulations. The Mission, Anti-mission, North, etc., faces all share similar temperature profiles throughout material simulations. This may allow for certain objects to be treated as a simple isothermal node having a certain orientation and location. RTE temperature appears to be independent of tumble rate for our chosen rates of 1, 0.1, and 0.01 rpm.

Further work will be done incorporating additional debris geometries such as flat plates, spheres, and other non-cuboid objects into this study. Studies will be done analyzing debris objects in a varying number of low-Earth orbits. Future analysis will be concerned with how the findings, conclusions, assumptions made regarding the thermal behavior of space debris may change due to the aforementioned variations of debris specifications.

ACKNOWLEDGEMENTS

This work was supported by the National Science Foundation under grants CNS-0959985, CNS-1042341, HRD-0833093, and IIP-1230661. The author of this paper was partially supported by the Department of Defense (DoD) through the National Defense Science & Engineering Graduate Fellowship (NDSEG) Program. Use of STK 10 was provided via the Educational Alliance Program partnership between Florida International University and Analytic Graphics Inc..

REFERENCES

- [1] Parliamentary Office of Science and Technology, *Space Debris* (2010). Postnote. Mar 2010 No 355, 1-4. Available at www.parliament.co.uk/post
- [2] Smith, Warren J. "Radiometry and Photometry." *Modern Optical Engineering: The Design of Optical Systems*. New York: McGraw-Hill, Ch.8. 2000.
- [3] John V. Lambert ; Thomas J. Osteen ; Butch Kraszewski; Determination of debris albedo from visible and infrared brightnesses. *Proc. SPIE 1951, Space Debris Detection and Mitigation*, 32 (September 15, 1993);
- [4] MATLAB 7.13, The MathWorks, Inc., Natick, Massachusetts, United States.
© 2013 The MathWorks, Inc. MATLAB and Simulink are registered trademarks of The MathWorks, Inc
- [5] Systems Tool Kit 10, Analytic Graphics Inc., Exton, Pennsylvania, United States.
© 2013 Analytical Graphics, Inc. All rights reserved. STK Systems Tool Kit® and Systems Tool Kit® are registered marks of Analytical Graphics, Inc.
- [6] Wyatt, Clair L.; *Electro-Optical System Design For Information Processing*. New York: McGraw-Hill, Ch. 4,8. 1991.
- [7] Gilmore, David G.; *Satellite Thermal Control Handbook*. El Segundo, CA: Aerospace Corporation, 1994.
Print